Pressure tensor for inhomogeneous fluids

B. D. Todd, Denis J. Evans, and Peter J. Daivis
Research School of Chemistry, Australian National University, Canberra, Australian Capital Territory 0200, Australia
(Received 8 September 1994; revised manuscript received 13 March 1995)

We develop a simple, efficient, and general statistical mechanical technique for calculating the pressure tensor of an atomic fluid. The method is applied to the case of planar Poiseuille flow through a narrow slit pore, and the results indicate that our technique is accurate and relatively efficient. A second method to calculate shear stress is derived from the momentum continuity equation. This mesoscopic method again is seen to be accurate with low statistical uncertainty. Using both approaches, the viscosity is calculated as a function of position across the pore, and is seen to oscillate because of a wall-induced local structure in the fluid. We discuss these methods in relation to the well-known ambiguity of the pressure tensor.

PACS number(s): 03.40.Gc, 02.50.−r, 51.10.+y, 05.70.Ln

I. INTRODUCTION

In this paper we give an alternative derivation of the Irving-Kirkwood [1] expression for the pressure tensor. Our derivation is valid for highly inhomogeneous, nonequilibrium fluids and avoids the mathematically awkward Taylor series expansion of differences in delta functions that is used in the Irving-Kirkwood [1] (IK) derivation. Our method also avoids the heuristic notion of the force "across" a unit area and is instead simply based on the continuity equations of hydrodynamics. We use our statistical mechanical expression to study the variation of the pressure tensor inside narrow slit pores. We also compare these results with those obtained by a simple integration of the momentum continuity equation. This latter method is mesoscopic in the sense that it is not based on any molecular hypothesis.

The pressure tensor of an atomic fluid $\mathbf{P}$ is often defined as the infinitesimal force $d\mathbf{F}$ felt across an infinitesimal area $d\mathbf{A}$, which moves with the local streaming velocity $\mathbf{u}(\mathbf{r},t)$ of the fluid

$$d\mathbf{F}=-d\mathbf{A}\cdot\mathbf{P}\ . \tag{1}$$

The pressure tensor can be written as a linear sum of kinetic, $\mathbf{P}^k$, and potential, $\mathbf{P}^u$, components. In (1), the kinetic component is deemed to be across the surface $d\mathbf{A}$ if at a time t, a particle moves through (or across) the surface. The potential component $\mathbf{P}^u$, due to intermolecular forces, is, however, not as easily defined. An interatomic force between two atoms is often said to be "across" the surface if the line between the centers of mass of the two atoms cuts through (or across) the surface defined by $d\mathbf{A}$. (This is the so-called Irving-Kirkwood convention [1].)

However, there is really no unambiguous definition of "across" for either the kinetic or the potential contributions to the pressure tensor. For example, there are obvious difficulties that arise in handling many-body force contributions to the potential part of the pressure tensor. Even for pair forces there is no unique way to determine exactly which molecular pairs contribute to $d\mathbf{F}$ [1–3]. Several different techniques have been developed to calculate the potential component of the pressure tensor; for example, those of Irving and Kirkwood [1] and Harasima [4].

The ambiguities in both components of the pressure tensor are perhaps best illustrated by the fact that the predictions of hydrodynamics are unaltered if we add the curl of an arbitrary vector field to the pressure tensor. In hydrodynamics it is only the *gradient* of the pressure tensor which appears in the equations of motion. Only variations in stress can cause acceleration of fluid elements.

The Irving-Kirkwood expression for the pressure tensor at time t [1,10] is

$$\mathbf{P}(\mathbf{r},t)=\frac{1}{V}\left[\sum_i m_i[\mathbf{v}_i(t)-\mathbf{u}(\mathbf{r}_i,t)][\mathbf{v}_i(t)-\mathbf{u}(\mathbf{r}_i,t)] + \tfrac{1}{2}\sum_{ij}\mathbf{r}_{ij}(t)O_{ij}(t)\mathbf{F}_{ij}(t)\big|_{\mathbf{r}_i(t)=\mathbf{r}}\right]\ . \tag{2}$$

In (2), V is the volume of the system, $\mathbf{v}_i$ is the total particle velocity, $\mathbf{u}$ is the streaming velocity of the fluid, $\mathbf{F}_{ij}$ is the force on atom i due to atom j, and O_{ij} is the differential operator,

$$O_{ij}=1-\frac{1}{2!}\mathbf{r}_{ij}\cdot\frac{\partial}{\partial\mathbf{r}}+\cdots+\frac{1}{n!}\left[-\mathbf{r}_{ij}\cdot\frac{\partial}{\partial\mathbf{r}}\right]^{n-1}+\cdots\ . \tag{3}$$

In the IK derivation the O_{ij} operator results [1] from an expansion of the difference of δ functions specifying atomic positions. If one is investigating the properties of bulk fluids subject to pair interactions, which have a uniform density, then the above expression with $O_{ij}=1$ is exact. We call the full Irving-Kirkwood expression for the pressure tensor the IK expression. We call the $O_{ij}=1$ approximation to the full expression the IK1 expression.

One of the main objectives of this paper is to obtain some quantitative understanding of the deviation of O_{ij}

from unity in inhomogeneous fluids close to walls. In principle, one could calculate the various O_{ij} terms, but this is neither algebraically simple nor computationally efficient.

There have been numerous equilibrium calculations of the pressure tensor in the liquid-gas interface, thereby enabling a determination of the surface tension of fluids, e.g., [5–9]. In the case of an equilibrium planar interface with surface area A, the Irving-Kirkwood definition of the pressure tensor leads to the following expressions for the transverse and normal components of $\mathbf{P}$, respectively [5,7]:

$$P_T(z)=\rho(z)kT-\frac{1}{4A}\left[\sum_{i<j}\frac{x_{ij}^2+y_{ij}^2}{r_{ij}}\phi'(r_{ij})\frac{1}{|z_{ij}|}\times\Theta\left[\frac{z-z_i}{z_{ij}}\right]\Theta\left[\frac{z_j-z}{z_{ij}}\right]\right], \tag{4}$$

$$P_N(z)=\rho(z)kT-\frac{1}{2A}\left[\sum_{i<j}\frac{z_{ij}^2}{r_{ij}}\phi'(r_{ij})\frac{1}{|z_{ij}|}\times\Theta\left[\frac{z-z_i}{z_{ij}}\right]\Theta\left[\frac{z_j-z}{z_{ij}}\right]\right], \tag{5}$$

where in these planar geometries x and y are parallel to the surface and z is perpendicular, $\rho(z)$ is the local density at z, $\phi(r_{ij})$ is the intermolecular potential, $\Theta(x)$ is the Heaviside step function, and $\mathbf{r}_{ij}=\mathbf{r}_i-\mathbf{r}_j$. Note: $P_T=P_{xx}=P_{yy}$ and $P_N=P_{zz}$. However, as they stand these equations are not valid for a nonequilibrium system.

The motivation for this work was to develop a general statistical mechanical technique for calculating the pressure tensor in narrow channels, bearing in mind the need for simplicity, generality, and computational efficiency. We apply the technique to the specific case of nonequilibrium planar Poiseuille flow, and show that it is an accurate and simple means by which the pressure tensor and local viscosity can be calculated. Furthermore, for this type of flow we develop a mesoscopic method to calculate P_{xy} from a solution to the momentum continuity equation of hydrodynamics and compare this result with our statistical mechanical technique. The accuracy and simplicity of both methods have implications for the case of fluid flows in microporous materials, and should be of use to engineers where experimental measurements of such local viscosities are difficult to perform, and previous theoretical work has been quite limited.

II. THEORY

A. Statistical mechanical expressions for the pressure tensor

Most derivations of the statistical mechanical form of the pressure tensor fall into two classes. They either make use of the machinery of equilibrium statistical mechanics and employ the thermodynamic relation, $p=-\partial A/\partial V|_T$, or its equivalent, or they make a direct mechanical calculation of the infinitesimal force $d\mathbf{F}$, that "acts across an infinitesimal co-moving area $d\mathbf{A}$," using definition (1). For our present purposes the thermodynamic route is inapplicable since we need to be able to compute the pressure tensor away from equilibrium. The second route is valid away from equilibrium but seems somewhat heuristic.

The IK derivation of (2) is based on the conservation laws of hydrodynamics and is valid for inhomogeneous nonequilibrium systems. However, the derivation of the O_{ij} expansion is unconvincing (it involves taking Taylor series expansions of the differences between δ functions) and the practical calculation of the O_{ij} expansion is computationally daunting.

In this paper we present an alternative derivation of the pressure tensor that, like the IK derivation, is based on the mass and momentum continuity equations of hydrodynamics. However, unlike IK we avoid the expansion of delta functions by carrying out much of the derivation in reciprocal space.

We begin by adopting the usual definition of the microscopic mass density, $\rho(\mathbf{r},t)\equiv\sum_i m\delta(\mathbf{r}-\mathbf{r}_i(t))$. This definition leads, using the mass continuity equation $\partial\rho/\partial t=-\nabla\cdot\mathbf{J}$, to the following equation for the momentum density $\mathbf{J}(\mathbf{r},t)$:

$$J_\alpha(\mathbf{r},t)\equiv\sum_i m v_{\alpha i}\delta(\mathbf{r}-\mathbf{r}_i(t)),\quad \alpha=x,y,z\ , \tag{6}$$

where $v_{\alpha i}$ is the laboratory velocity of particle i. Because the mass continuity equation refers only to the divergence of $\mathbf{J}$ and not to the momentum density itself, we can add the curl of any vector field to $\mathbf{J}$ without any observable effect on the mass continuity equation. This is an elementary example of a gauge transformation.

Since we shall be interested in planar interfaces with a normal parallel to, say, the y axis, it is convenient to consider a partial Fourier transform over the y coordinate,

$$J_\alpha(k_y,x,z)\equiv\int_{-\infty}^{+\infty}\sum_i m v_{\alpha i}\delta(\mathbf{r}-\mathbf{r}_i)e^{ik_y y}dy=\sum_i m v_{\alpha i}\delta(x-x_i)\delta(z-z_i)e^{ik_y y_i}\ . \tag{7}$$

If the fluid is assumed to be uniform in the x,z directions we can average over them and write the transformed momentum density as

$$J_\alpha(k_y)=\frac{1}{A}\sum_i m v_{\alpha i}e^{ik_y y_i}\ , \tag{8}$$

where A is the magnitude of the area that has as its normal the y axis.

Now for any fluid, no matter how inhomogeneous and no matter how far from equilibrium, the rate of change of the momentum density is related to the divergence of the pressure tensor $\mathbf{P}$,

$$\frac{\partial\mathbf{J}(\mathbf{r},t)}{\partial t}=-\nabla\cdot[\mathbf{P}(\mathbf{r},t)+\rho(\mathbf{r},t)\mathbf{u}(\mathbf{r},t)\mathbf{u}(\mathbf{r},t)]\ , \tag{9}$$

where $\mathbf{u}(\mathbf{r},t)$ is the streaming velocity of the fluid. This equation says that momentum is conserved and in any relaxation process can only redistribute itself (i.e., no

sources or sinks). It also shows, as mentioned in the Introduction, that (like the momentum density) **P** is not uniquely defined and that one can apply a gauge transformation without changing the rate of change of the momentum density.

In k space the momentum continuity equation is

$$\frac{\partial J_\alpha(k_y)}{\partial t}=ik_y[P_{\alpha y}(k_y)+\tilde{f}(\rho(y)u_\alpha(y)u_y(y))] , \quad (10)$$

where we note here that $\tilde{f}(\ )$ denotes the Fourier transform of the quantity in brackets. Substituting (8) into (10) gives the potential contribution to the wave-vector-dependent pressure tensor as

$$P^U_{\alpha y}(k_y)=\frac{1}{A}\sum_i \frac{F_{\alpha i}}{ik_y}e^{ik_y y_i} , \quad (11)$$

while the kinetic contribution is

$$P^K_{\alpha y}(k_y)=\frac{1}{A}\sum_i \frac{m v_{\alpha i}}{ik_y}\frac{d}{dt}e^{ik_y y_i}-\tilde{f}(\rho u_\alpha u_y) . \quad (12)$$

In Ref. [10] we showed that Eqs. (11) and (12) for the wave-vector-dependent pressure tensor are Fourier transforms of the Irving-Kirkwood expression (2), including the infinite order expansion of the O_{ij} operator. We will now find simple, equivalent real-space expressions to (2). These expressions also have the Irving-Kirkwood gauge, and also include the full O_{ij} operator expansion.

We make an inverse Fourier transform of the configurational component of the pressure tensor (11), to find that

$$P^U_{\alpha y}(y)=\frac{1}{2\pi A}\int_{-\infty}^{+\infty}\sum_i \frac{F_{\alpha i}}{ik_y}e^{ik_y y_i}e^{-ik_y y}dk_y . \quad (13)$$

Utilizing the fact that

$$\frac{1}{\pi}\int_{-\infty}^{\infty}\frac{\exp(iky)}{ik}dk=\mathrm{sgn}(y) , \quad (14)$$

it is trivial to show

$$P^U_{\alpha y}(y)=\frac{1}{2A}\sum_i F_{\alpha i}\mathrm{sgn}(y_i-y) . \quad (15)$$

If we let $\mathbf{F}_{ij}$ be the force on particle i due to particle j, we can symmetrize this expression as

$$\begin{aligned}P^U_{\alpha y}(y)&=\frac{1}{4A}\sum_{ij}F_{\alpha ij}[\mathrm{sgn}(y_i-y)-\mathrm{sgn}(y_j-y)]\\&=\frac{1}{4A}\sum_{ij}F_{\alpha ij}[\Theta(y_i-y)\Theta(y-y_j)\\&\qquad-\Theta(y_j-y)\Theta(y-y_i)] , \end{aligned}\quad (16)$$

where Θ denotes the Heaviside step function.

Since $\mathbf{F}_{ij}=-\mathbf{F}_{ji}$, if y_i, y_j are both either smaller or larger than y, both Heaviside products are zero and the contribution to the pressure tensor is zero. If $y_i<y$ and $y_j>y$ then the first product of step functions is zero while the second is unity. If $y_i>y$ and $y_j<y$ then the second product is zero while the first is unity. Thus (16) denotes the intermolecular "force across unit area." Since the sum is an unrestricted double sum every i,j pair is counted twice; hence the extra factor of 2 in the denominator. Finally we note that one can show the formal equivalence of (16) with the configuration part of (2).

The kinetic part of the pressure tensor can be obtained using similar methods. From (12), we see that

$$\begin{aligned}P^K_{\alpha y}(y)&=\frac{1}{2\pi A}\int_{-\infty}^{+\infty}dk_y\sum_i\frac{m v_{\alpha i}}{ik_y}\frac{d}{dt}\exp[ik_y(y_i-y)]\\&\qquad-\rho u_\alpha u_y .\end{aligned}\quad (17)$$

If we interchange the order of integrating with respect to k_y and differentiating with respect to time we find

$$\begin{aligned}P^K_{\alpha y}(y)&=\frac{1}{2\pi A}\sum_i m v_{\alpha i}\frac{d}{dt}\int_{-\infty}^{+\infty}dk_y\frac{\exp[ik_y(y_i-y)]}{ik_y}\\&\qquad-\rho u_\alpha u_y\\&=\frac{1}{2A}\sum_i m v_{\alpha i}\frac{d}{dt}\mathrm{sgn}(y_i-y)-\rho u_\alpha u_y .\end{aligned}\quad (18)$$

In obtaining the second of these equalities we have used (14). In Eq. (18) we note that we only obtain nonzero contributions to the kinetic component of the pressure tensor when particles cross the plane. If particles remain on either side of the plane $d\ \mathrm{sgn}(y_i-y)/dt=0$.

Applying chain rule differentiation to the sgn function, we obtain

$$\begin{aligned}P^K_{\alpha y}(y)&=\frac{1}{2A}\sum_i m v_{\alpha i}v_{yi}\frac{d}{dy}\mathrm{sgn}(y_i-y)-\rho u_\alpha u_y\\&=\frac{1}{A}\sum_i m v_{\alpha i}v_{yi}\delta(y_i-y)-\rho u_\alpha u_y .\end{aligned}\quad (19)$$

Equation (19) may be rewritten in terms of peculiar momenta $\mathbf{p}_i$ by use of the microscopic definitions of the mass and momentum density,

$$P^K_{\alpha y}(y)=\frac{1}{A}\sum_i\frac{p_{\alpha i}p_{yi}}{m}\delta(y_i-y) . \quad (20)$$

We note now that (20) is the usual Irving-Kirkwood expression for the kinetic part of the pressure tensor.

If particle i crosses the plane at a set of times $\{t_{i,m};i=1,\ldots,N;m=1,2,\ldots\}$ and if we use the sign of the y component of the momentum to tell whether the crossing is from right to left or vice versa, (20) can be written as

$$\begin{aligned}P^K_{\alpha y}(y,t)&=\frac{1}{2A}\sum_i p_{\alpha i}(t)\frac{d}{dt}\mathrm{sgn}[y_i(t)-y]\\&=\frac{1}{A}\sum_{t_{i,m}}\sum_i p_{\alpha i}(t_{i,m})\delta(t_{i,m}-t)\mathrm{sgn}[p_{yi}(t_{i,m})] .\end{aligned}\quad (21)$$

The time-averaged kinetic component of the pressure tensor can therefore be written as

$$P^K_{\alpha y}(y)=\lim_{\tau\to\infty}\frac{1}{A\tau}\sum_{0<t_{i,m}<\tau}\sum_i p_{\alpha i}(t_{i,m})\mathrm{sgn}[p_{yi}(t_{i,m})]\ . \tag{22}$$

From Eqs. (16) and (22) we can easily see that the pressure tensor can indeed be identified as that part of the "force that acts across a unit area." Our derivation does not require any assumptions regarding *when* an interparticle force $\mathbf{F}_{ij}$ is "across" a plane. Neither does it involve Taylor series expansions of differences of δ functions. Our derivation removes these difficulties and replaces them with the well-defined mathematical procedure of setting the gauge of both the pressure tensor and the momentum density. We note that while the procedure of working in k space greatly facilitates formal manipulation of the mathematics, it does not remove the basic conceptual problems associated with the O_{ij} operator in real space.

The difference between the full IK and the approximate IK1 expressions for the configurational components of the pressure tensor may be seen more readily by noting their instantaneous k-space expressions. The IK expression is given as

$$\mathbf{P}^U_{\mathrm{IK}}(\mathbf{k})=-\frac{1}{2}\sum_{ij}\mathbf{r}_{ij}\mathbf{F}_{ij}\left[\frac{1-e^{i\mathbf{k}\cdot\mathbf{r}_{ij}}}{-i\mathbf{k}\cdot\mathbf{r}_{ij}}\right]e^{i\mathbf{k}\cdot\mathbf{r}_i}\ , \tag{23}$$

whereas the simpler IK1 approximation is

$$\mathbf{P}^U_{\mathrm{IK1}}(\mathbf{k})=-\tfrac{1}{2}\sum_{ij}\mathbf{r}_{ij}\mathbf{F}_{ij}e^{i\mathbf{k}\cdot\mathbf{r}_j}\ . \tag{24}$$

As we shall see, Eqs. (16) and (22) are quite useful in numerical calculations of the pressure tensor. Although they have rarely been used in the past they have two very desirable properties: they incorporate the full Irving-Kirkwood O_{ij} operator expansion and they have high numerical efficiency. The first of these properties means that these expressions can be used in interfaces and narrow pores. The second property means that they produce high accuracy results with comparatively little computational effort. We call the determination of the pressure tensor by (16) and (22), the method of planes, MOP for short.

B. Determination of the pressure tensor from the continuity equation and molecular dynamics

Consider the momentum conservation equation for a fluid in which each particle is subject to an external field $\mathbf{F}_e$ [10,11], and the fluid is subject to a pressure gradient ∇p,

$$\rho(\mathbf{r},t)\frac{d\mathbf{u}(\mathbf{r},t)}{dt}=-\nabla\cdot\mathbf{\Pi}-\nabla p+n(\mathbf{r},t)\mathbf{F}_e\ . \tag{25}$$

In this equation $\mathbf{u}(\mathbf{r},t)$ is the fluid streaming velocity at position $\mathbf{r}$ and time t, $\rho(\mathbf{r},t)$ the mass density at $\mathbf{r}$ and t, $n(\mathbf{r},t)$ the number density, and $\mathbf{\Pi}$ the viscous pressure tensor (i.e., $\mathbf{\Pi}=\mathbf{P}-p\mathbf{1}$, where $\mathbf{P}$ is the pressure tensor and p the hydrostatic pressure). It is the pressure *gradient* which drives the flow. The actual value of the pressure is not directly relevant. The pressure is only important insofar as it determines the thermodynamic state of the flowing fluid. The fluid therefore cannot distinguish between a situation where the flow is driven by a pressure gradient ∇p or by an external field. If we choose an external field such that

$$\nabla p=-n(\mathbf{r},t)\mathbf{F}_e\ , \tag{26}$$

we can study the flow properties of the system in the absence of an actual pressure gradient.

In computer simulations, the advantage of using an external field to drive the flow rather than an actual pressure gradient is that under a constant external field the system can remain longitudinally homogeneous. Under an actual pressure gradient this is not possible because in compressible fluids pressure gradients imply density gradients. In real experiments these density gradients are usually so small that they are unobservable. However, in order to achieve satisfactory signal-to-noise ratios, computer simulations need to employ very large macroscopic values for the pressure gradient. These large gradients would lead to significant density variations over the length of the simulation cell. Such variations would be incompatible with periodic boundary conditions, which are the desirable boundary conditions for computer simulations because they minimize the effects of boundaries.

A possible objection to our external field method may be that in (26), the pressure gradient that is equivalent to the external field is not constant. Since the field is constant but (particularly near the walls) the density is a function of position, the equivalent pressure gradient is not constant. This would seem to be at variance with the standard text book description of Poiseuille flow. We have two answers to this objection: First, in the weak-field limit the fluid's material properties are independent of whether the field is constant or inversely proportional to density. The results of these two *different* experiments are processed differently, leading to identical material properties in the weak-field limit. Second, in an actual Poiseuille flow experiment where the walls are only a few molecular diameters apart, it is not true that the pressure gradient is necessarily independent of position across the channel.

Consider a gravity-driven flow between closely spaced parallel plates whose normals are perpendicular to the direction in which gravity acts. In this case the equation of motion is

$$\rho(\mathbf{r},t)\frac{d\mathbf{u}(\mathbf{r},t)}{dt}=-\nabla\cdot\mathbf{\Pi}+n(\mathbf{r},t)\mathbf{F}_e\ , \tag{27}$$

where the magnitude of the external field $\mathbf{F}_e$ is simply the molecular mass of the fluid particles m multiplied by the acceleration due to gravity g. In writing (27) we have assumed that the vertical height of the plates is sufficiently small that the difference in atmospheric hydrostatic pressure between the top and bottom of the plates may be ignored. Equation (27) shows that for gravity-driven flow in a narrow slit pore, the effective pressure gradient appearing in (26) is *not* constant across the slit, but rather is proportional to the number density across the pore.

In order to solve (27) we consider a three-dimensional system where a fluid is sandwiched between two parallel planar walls. We define the geometry such that the flow is in the x direction, $\mathbf{F}_e = \mathbf{i}F_e$, with the walls separated by a length L_y in the y direction, as is shown in Fig. 1. If we neglect the roughness of the walls, then periodic boundary conditions ensure that our system is invariant in the x,z directions, and $\Pi = \Pi(y)$ and $n(\mathbf{r}) = n(y)$. We first examine the left-hand side of (27) and expand the total derivative,

$$\frac{d\mathbf{u}(\mathbf{r},t)}{dt} = \frac{\partial \mathbf{u}(\mathbf{r},t)}{\partial t} + \mathbf{u}\cdot\nabla\mathbf{u} \ . \tag{28}$$

At low Reynolds' number we note $\partial \mathbf{u}(\mathbf{r},t)/\partial t = \mathbf{0}$, $u_x = u_x(y)$, $u_y = u_z = 0$, and hence $d\mathbf{u}(\mathbf{r},t)/dt = \mathbf{0}$.

We now consider the right-hand side of Eq. (27) and observe that again we are only interested in the x components of the vector quantities. Π is a second-rank tensor, and noting that $\Pi = \Pi(y)$, we have $(\nabla\cdot\Pi)_x = \partial \Pi_{xy}/\partial y$. Thus Eq. (27) reduces to

$$\frac{\partial \Pi_{xy}}{\partial y} = n(y) F_e \ . \tag{29}$$

The solution to (29) is

$$\Pi_{xy} = A_1(y) + A_0 \ , \tag{30}$$

where $A_1(y) = F_e \int_{-l_y/2}^{y} dy' \, n(y')$. A_0 is an arbitrary integration constant and l_y is the effective length of the channel accessible to the fluid, which is defined later in Sec. III B.

Since $n(y)$, the number density, can easily be obtained from simulation, Eq. (30) gives us an independent mesoscopic route to the shear stress. This route is termed "mesoscopic" since it is independent of molecular considerations. Unlike the IK, IK1, or MOP methods, this mesoscopic method is valid for fluids in which the constituent atoms are subject to many-body forces.

The constant A_0 is arbitrary and shifts the entire Π_{xy} profile by an additive constant. The simplest assumption we can make in choosing this constant is that it is zero when the strain rate is zero, $\Pi_{xy}(y=0) = 0$, and therefore

$$A_0 = -\frac{1}{l_y} \int_{-l_y/2}^{l_y/2} A_1(y) dy \ . \tag{31}$$

The assumption that in the middle of the flow where the strain rate is zero, the shear stress is also zero, sets the gauge for the shear stress. We made exactly the same assumption in choosing the gauge for our statistical mechanical expressions for the pressure tensor [i.e., in going from (10) to (11) and (12)]. As already noted, this gauge is identical to the Irving-Kirkwood gauge. We call the determination of the pressure tensor by integrating the momentum conservation equation the IMC method.

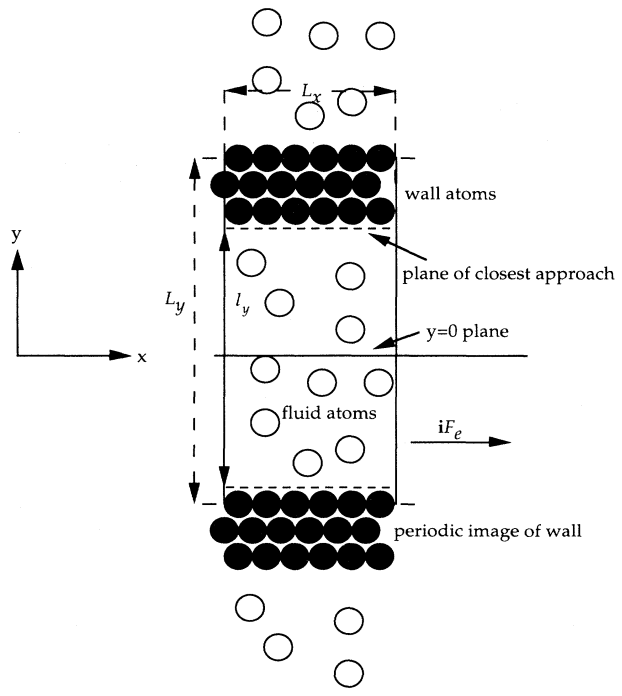

FIG. 1. Simulation geometry for planar Poiseuille flow. The z axis is normal to the page.

III. SIMULATION OF POISEUILLE FLOW

A. Equations of motion

Figure 1 describes the geometry of the system. We ran simulations consisting of 558 fluid atoms and 54 wall atoms. The interatomic potential function $\phi(r)$ was the Weeks-Chandler-Anderson (WCA) potential, [12]: $\phi(r) = 4(r^{-12} - r^{-6}) + 1$ for $r < 2^{1/6}$; $\phi(r) = 0$ for $r > 2^{1/6}$ (we have defined the WCA potential constants σ and ε to be unity for simplicity; we also note that the atomic mass has been set to unity). The walls are three atomic layers thick (18 atoms per layer) and are fixed in place in an fcc lattice structure by a combination of harmonic restoring forces and a constraint mechanism. The simulation cell is periodic in all three dimensions. There is only one three-atom-thick wall per simulation cell. The second wall is simply the periodic image of the first wall. This periodicity also ensures that the total density of the system remains constant.

We use a simple harmonic tethering potential to confine wall atoms to the neighborhood of their nominated lattice sites. Following Powles, Murad, and Ravi [13] the restoring potential applied to each wall atom is just

$$\phi_{Ti} = \tfrac{1}{2} K (\mathbf{r}_i - \mathbf{r}_{ei})^2 \ , \tag{32}$$

where $\mathbf{r}_{ei}$ is the equilibrium site of atom i, and K is a spring constant. This tethering potential is additional to the usual wall-wall and wall-fluid WCA interatomic interactions.

Liem, Brown, and Clarke [14] used a similar simulation arrangement in their boundary driven shear studies. They also used the restoring potential of Powles, Murad, and Ravi. (Unlike us, they did not use periodicity in the y direction.)

However, they found that the fluid pressure was sufficient to cause a slight increase in the wall separation.

Furthermore, such an effect is expected to be dependent on the average flow velocity of the fluid and hence is not desirable because it means that the system volume and average density do not remain constant during a simulation. This is especially undesirable when studying small pore widths, where even a slight increase in the volume can have a significant effect on the density of the fluid. In order to remove this difficulty we have developed a constraining mechanism, based on Gauss's principle of least constraint [10], which keeps the center of mass of *each* of the atomic wall layers constant.

The constraint we impose is that the y coordinate of the center of mass of *each* of the three wall layers, L_i: $i=1,2,3$, remains constant. We assume that each layer contains N_w particles and that there are therefore a total of $3N_w$ wall atoms.

Since Poiseuille flow involves a steady-state flow of fluid, we require a method of removing viscous heat that is produced in the fluid. Again we invoke Gauss' principle of least constraint to maintain the walls at a constant temperature. Thus excess heat will be removed from the fluid by heat conduction from the fluid to the thermostated walls. The technique is well known [10], and we write down only the final form of the thermostated equations of motion.

The equations of motion for the wall particles are

$$\dot{\mathbf{r}}_i=\mathbf{p}_i/m \ , \qquad \dot{\mathbf{p}}_i=-K(\mathbf{r}_i-\mathbf{r}_{ei})+\sum_{j=1}^{N}\mathbf{F}_{ij}-\alpha\mathbf{p}_i-\mathbf{j}\lambda_{L_j} \ , \quad i\in L_i \ . \tag{33}$$

The layer multipler λ_{L_j} and the thermostat multiplier α are given by

$$\lambda_{L_j}=\frac{\mathbf{j}}{N_w}\cdot\sum_{i\in L_j}^{N_w}\left[-K(\mathbf{r}_i-\mathbf{r}_{ei})+\sum_{k=1}^{N}\mathbf{F}_{ik}\right] , \qquad \text{where } \sum_{L_j=1}^{3}\sum_{i\in L_j}^{N_W}1=3N_w \ ,$$

$$\alpha=\frac{\displaystyle\sum_{i\in L}^{3N_w}\left\{\left[-K(\mathbf{r}_i-\mathbf{r}_{ei})+\sum_{j=1}^{N}\mathbf{F}_{ij}-\mathbf{j}\lambda_{L_i}\right]\cdot p_i\right\}}{\displaystyle\sum_{i\in L}^{3N_w}\mathbf{p}_i^2} \ . \tag{34}$$

Since there is no streaming motion of the wall particles in any direction, there is no difficulty in distinguishing between laboratory and peculiar momenta for the wall particles: the two momenta are identical.

The fluid particles obey Newton's equations of motion,

$$\dot{\mathbf{r}}_i=\mathbf{p}_i/m \ , \qquad \dot{\mathbf{p}}_i=\sum_{j=1}^{N}\mathbf{F}_{ij}+\mathbf{i}F_e \ , \tag{35}$$

where $\mathbf{F}_{ij}$ is the total WCA force on atom i due to both fluid-fluid and fluid-wall interatomic interactions, and $\mathbf{i}F_e$ is the external driving force described in Sec. II. It is understood that $\mathbf{p}_i$ is the *laboratory* momentum of particle i (i.e., the sum of the peculiar and streaming components).

B. General simulation considerations

The simulations were conducted using a fifth-order Gear predictor-corrector scheme with an integration time step of $\tau=0.001$. The fluid atoms were initially arranged in an fcc structure and the system allowed to reach steady state before data were taken. Simulations were carried out at two different number densities, $\bar{n}=N/V=0.4181$ and 0.8362. However, it is not clear how to determine the *average* density of a fluid because there is no unambiguous definition of the total volume that is accessible to the fluid.

We denote the unit-cell dimensions as L_x,L_y,L_z. The values of L_x,L_y,L_z were 7.4217, 26.1269, 7.4217 for the lower density and 5.2479, 26.5625, 5.2479 for the higher. It is important to note that L_y includes the fluid and wall particles (see Fig. 1). For simplicity we make the $y=0$ plane midway between the walls. To judge what would be the *accessible* width of the pore l_y we examined the fluid density profile as a function of y and measured the width from those points where $n(y)>0.1$, which we arbitrarily define as the "plane of closest approach." Below this value, $n(y)$ drops to zero very rapidly. For both densities this gave a value of $l_y=24.23$.

Simulations for $\bar{n}=0.8362$ were carried out with $F_e=0.05$ and an optimal wall force constant of $K=57.15$ (see Liem, Brown, and Clarke [14]), while for $\bar{n}=0.4181$, $F_e=0.01$ and $K=100$. The value of K for the latter case, though not optimal for heat transfer, was higher because it was found that fluid atoms penetrated the walls relatively frequently at this lower fluid density; hence the walls needed to be "harder" to prevent this penetration. However, one must be careful not to use too high a value of K as this will make the equations of motion stiff and also reduce heat transfer between fluid and wall atoms, allowing the fluid to heat up. Both simulations were run at a constant wall temperature of 0.722, and the wall densities were 1.2549 and 0.8700 for the fluid densities of 0.8362 and 0.4181, respectively, where the wall density is here defined as $3N_w/(L_xL_z\Delta y_w)$, and Δy_w is the wall thickness (1.5625 and 1.1269 for high and low densities, respectively). Once steady state was achieved several runs of 100 000 time steps were undertaken for each density and averages taken of the quantities of interest.

Because of the streaming motion of the fluid, we must distinguish between the peculiar and laboratory velocities of the fluid particles. The kinetic component of any thermodynamic quantity, such as temperature or the kinetic components of the pressure tensor, must be calculated using the peculiar velocities $\mathbf{c}_i=\mathbf{v}_i-\mathbf{u}(y_i)$, where $\mathbf{v}_i$ is the laboratory velocity of particle i and $\mathbf{u}(y_i)$ is the streaming velocity at y_i. Here $\mathbf{u}(y)=\mathbf{i}u(y)$ because the driving force acts only in the x direction.

To determine the streaming velocity, at each time step we fit a sixth-order symmetric polynomial to the streaming velocity profile within the simulation and subtract this velocity from the laboratory velocity before calculat-

ing any thermodynamic kinetic quantities. In the zero-flow-rate limit, Navier-Stokes hydrodynamics predicts that the velocity profile is a quadratic function of separation [15]. For small slit pores this is expected to be incorrect because of steric effects near the walls.

The pressures calculated using our method of planes, described in Sec. II A, may be compared with those calculated from the Irving-Kirkwood real-space expression, (2), with $O_{ij}=1$ (i.e., IK1). We note that IK1 involves summations over a volume V. To find pressures as a function of y we thus need to divide the fluid region into bins, each of which has a volume $V_{\rm bin}=L_xL_z\Delta y$, where L_x, L_z are the lengths of the simulation box in the x and z directions, respectively, and Δy is the width in the y direction of each bin. The IK1 pressure tensor, as a function of y, measured in each bin will then be

$$\mathbf{P}_{\rm bin}(y,t)=\frac{1}{V_{\rm bin}}\left[\sum_{i\in{\rm bin}}[\mathbf{v}_i-\mathbf{i}u(y)][\mathbf{v}_i-\mathbf{i}u(y)]+\tfrac{1}{2}\sum_{\substack{ij\\ i\in{\rm bin}}}\mathbf{r}_{ij}\mathbf{F}_{ij}|_{y_i=y}\right], \tag{36}$$

where now the sum over i includes only atoms that are contained within the bin, and the sum over j includes all possible atoms within or outside the bin.

We can also calculate other quantities as a function of y by summing them over bins, such as the velocity, temperature, and density. In this way we can build up profiles of the various quantities of interest.

The viscosity can be calculated for each of the three methods described in Secs. I and II (IK1, MOP, and IMC), and is given by

$$\eta(y)=\lim_{F_e\to 0}-\frac{\langle P_{xy}(y)\rangle}{\gamma(y)}, \tag{37}$$

where $\gamma(y)$ is the y-dependent shear rate,

$$\gamma(y)=\frac{\partial u_x(y)}{\partial y}. \tag{38}$$

One can also determine an average viscosity (i.e., an average viscosity over the entire fluid region) $\bar{\eta}$ directly from continuum hydrodynamics. If one assumes the fluid is a uniform continuum with a constant density $\bar{n}$ and viscosity throughout the fluid (neither of which is strictly true), then in our coordinate system the streaming velocity profile derived from the Navier-Stokes equation is

$$u_x(y)=-\frac{\bar{n}F_e}{2\bar{\eta}}\left[y^2-\frac{l_y^2}{4}\right]. \tag{39}$$

Equation (39) with a second-order symmetric polynomial

$$u_x(y)=c_2y^2+c_0 \tag{40}$$

gives for the continuum viscosity

$$\bar{\eta}=-\frac{\bar{n}F_e}{2c_2}. \tag{41}$$

c_2 is obtained by fitting the simulated streaming velocity profile with (40). We will call this estimate of viscosity the continuum hydrodynamic viscosity, or CH for short.

Finally, for MOP it is a relatively simple matter to calculate the configurational part of the pressure tensor given by (16). One simply sums all $\mathbf{F}_{ij}$ terms such that atoms i and j are on opposite sides of the plane of interest. The plane may be *any* x-z plane in *any* region of the fluid, not just the wall-fluid interface. The kinetic contributions, described by (22), also are straightforward to compute; however, we note that any intersection of an atom with a plane will occur in a time $\leq\tau$. We interpolate the time at which this intersection occurs by a standard Newton-Raphson method.

IV. RESULTS

In order to verify the validity of the results we performed a number of standard equilibrium molecular dynamics (EMD) simulations of the bulk WCA fluid at constant temperature and volume (hence density), which corresponded to the appropriate average values of the temperature and density measured for the Poiseuille flow simulations. The standard EMD simulations were performed on a system of 540 fluid particles with three-dimensional periodicity. Table I displays the energy per particle and the pressure for the Poiseuille flow simulations at $\bar{n}=0.8362$ and 0.4181 ($\bar{T}=0.97$ and 0.86, respectively), and compares them with the energy per particle and pressure at the same values of $\bar{n}$ and $\bar{T}$ for the EMD bulk liquid simulations. Note that the pressure given for the Poiseuille flow simulations is actually P_{yy} averaged over 260 planes (the number planes used in our simulations) in the liquid. The plane separation was 0.09615. As can be seen, the results for both densities are in good agreement with each other and are within the range of errors. The fact that the thermodynamic properties such as internal energy and pressure are insensitive to the value

TABLE I. Comparison of internal energy per particle, $\bar{E}/N$, and pressure for nonequilibrium planar Poiseuille flow and bulk equilibrium molecular dynamics (EMD) at both densities used for this work. The temperatures quoted for the Poiseuille flow simulations are the overall average temperatures of the liquid systems studied, while the temperatures of the bulk EMD simulations were kept constant at the average temperatures of the Poiseuille flow systems by using a Gaussian thermostat. Note that for $F_e\neq 0$, $P\equiv\bar{P}_{yy}$.

Quantity	Poiseuille flow	Equilibrium bulk
	$\bar{T}=0.97$, $\bar{n}=0.8362$	
$\bar{E}/N$	2.34±0.02	2.361±0.002
P	7.52±0.04	7.514±0.009
F_e	0.05	0
	$\bar{T}=0.86$, $\bar{n}=0.4181$	
$\bar{E}/N$	1.45±0.02	1.453±0.001
P	1.02±0.01	1.015±0.003
F_e	0.01	0

TABLE II. P_{xx}, P_{yy}, and P_{zz} calculated for the overall Poiseuille flow system using the IK1 approximation.

Quantity	Poiseuille flow NEMD
	$\bar{T}=0.97$, $\bar{n}=0.8362$
P_{xx}	7.64±0.04
P_{yy}	7.76±0.04
P_{zz}	7.64±0.05
	$\bar{T}=0.86$, $\bar{n}=0.4181$
P_{xx}	1.03±0.02
P_{yy}	1.06±0.02
P_{zz}	1.03±0.02

of the external field implies that we are close enough to equilibrium for the assumption of local thermodynamic equilibrium to hold.

Table II shows the corresponding average values of P_{xx}, P_{yy}, and P_{zz} determined for the Poiseuille flow simulations using IK1, where here we have summed kinetic and potential components over the entire volume of the liquid system. Not surprisingly the pressures for both densities are slightly higher than the bulk simulations, because of the neglect of the O_{ij} terms in evaluating IK1. The P_{yy} components are also slightly higher than the corresponding P_{xx} and P_{zz} values.

For our system to be both mechanically stable and time independent, P_{yy} must be constant throughout the fluid. Figure 2 shows a comparison of P_{yy} as a function of y, calculated by both MOP and IK1, where $\Delta y=0.09615$. Two features of our MOP method stand out as significant: first, P_{yy} is indeed seen to be constant across the pore, and second, the relative accuracy of MOP is much greater than that of IK1. Both sets of results were obtained from exactly the same simulation data. The only difference is in how those data are processed.

We can go some way towards understanding the superior statistical efficiency of our MOP method. In the binned IK1 method the number of particles within each bin is proportional to the bin volume. In order to resolve the expected spatial variations of the pressure tensor as a function of position within the channel one needs at least ten bins or planes per particle diameter. As that volume goes to zero the variance of the IK1 pressure diverges as the reciprocal of the bin volume. On the other hand, in the MOP method the pressure computed across each plane is independent of the number or the spacing of other planes. This makes the MOP method very useful for carrying out high-resolution studies of the pressure tensor in confined geometries.

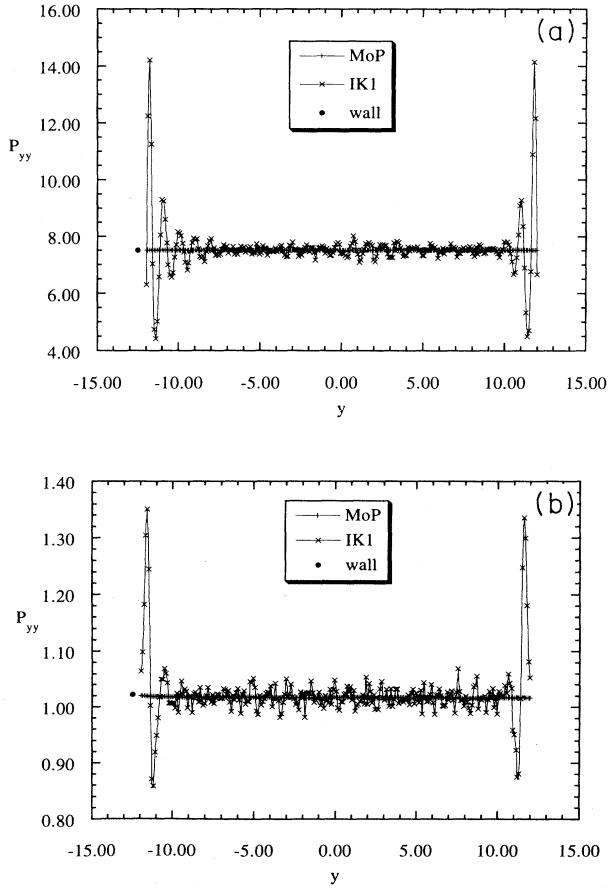

FIG. 2. P_{yy} calculated by IK1 and MOP. (a) $\bar{n}=0.8362$; (b) $\bar{n}=0.4181$.

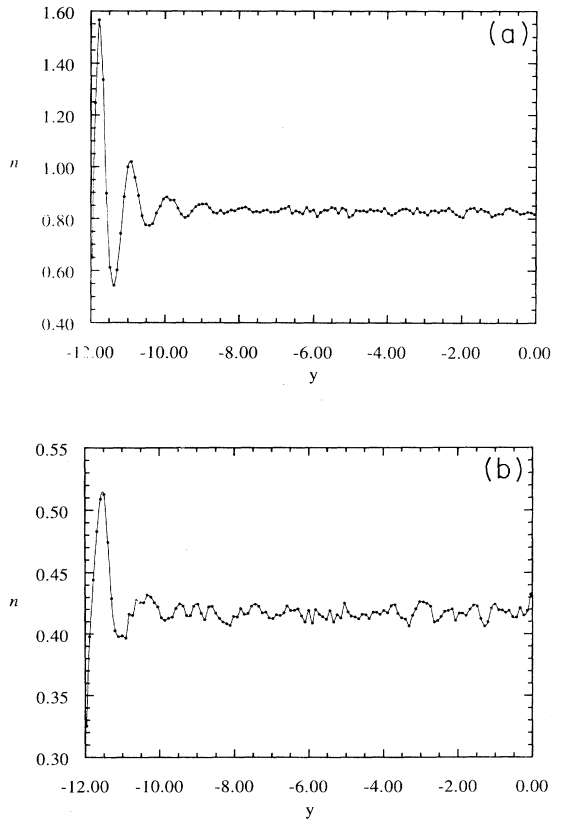

FIG. 3. Symmetrized number density profiles. (a) $\bar{n}=0.8362$; (b) $\bar{n}=0.4181$.

The IK1 method shows anomalies in P_{yy} near the walls, where P_{yy} begins to oscillate rapidly and with large amplitude. Again this is an artifact of neglecting to use the O_{ij} terms in the IK expression. The exclusion of these terms fails to correctly account for a correlation between P_{yy} and the pair distribution function. This correlation can be more easily seen in Figs. 3 and 4 by noting that the rapid oscillations in P_{yy} are observed in regions where rapid oscillations in the density profile occur. We note that because of spatial symmetry around $y=0$, the data in both figures have been symmetrized to improve the statistics.

Figure 2 also shows the value of P_{yy} measured at the left-hand wall of the system. This is defined simply as the total y force per unit area, exerted on the wall atoms by fluid particles on one side of the wall. Because of periodicity, the total force exerted on the wall by fluid particles on both sides of the wall is zero. The wall estimate for P_{yy} must of course agree with P_{yy} anywhere within the liquid, and once again we see that MOP verifies this quite accurately.

Of somewhat greater interest is the P_{xy} component of the pressure tensor, because it is through this component that we can calculate viscosity as a function of y throughout the liquid. In this work the P_{xy} components are calculated by four independent methods: IK1, MOP, via the integration of the momentum continuity equation (30), referred to as the IMC method, and finally by computing the shear stress on the wall, which is the total x force per unit area, exerted on the all atoms by fluid particles in one side of the wall.

Figure 5 shows P_{xy} calculated by IK1, MOP, and at the walls for both densities used in our simulations. Once again we see poor statistics and large oscillations in P_{xy} near the walls for the IK1 method. MOP once again displays significantly better statistics and is in good agreement with P_{xy} measured at the walls.

The IMC technique of calculating the pressure tensor is also in good agreement with MOP to within 3%. This is seen more readily in Fig. 6, where P_{xy} is plotted for both methods only for a distance of 3 atomic diameters from the left-hand wall. In Fig. 6(a) we see that for both the MOP and IMC techniques there are small oscillations in P_{xy} close to the wall. These do in fact extend towards the center of the pore, but are two weak to be seen on the scale of this figure. These oscillations are real effects. They are not to be confused with the large oscillations observed with the IK1 method, which are an anomalous consequence of setting $O_{ij}=1$.

In Fig. 7 we display the corresponding results for a

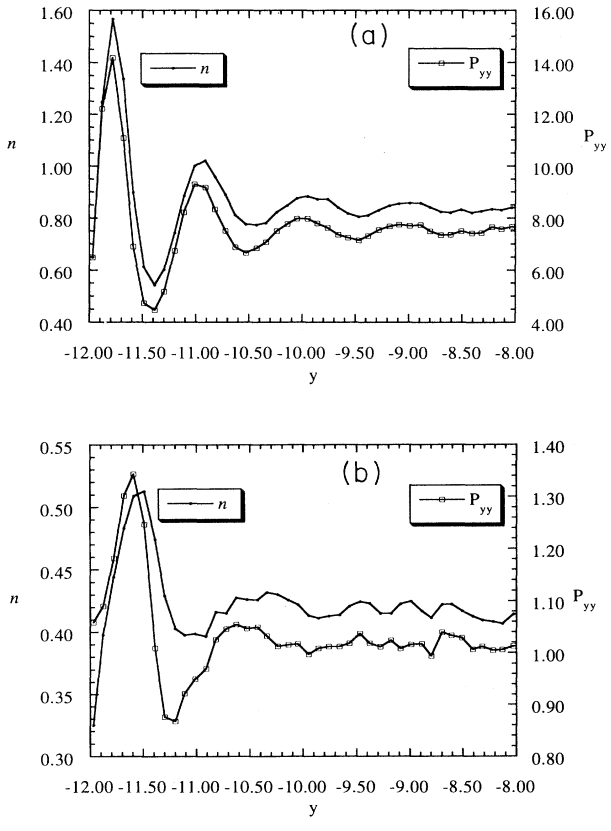

FIG. 4. Correlation between P_{yy} (IK1) and $n(y)$. (a) $\bar{n}=0.8362$; (b) $\bar{n}=0.4181$. Both P_{yy} and $n(y)$ profiles have been symmetrized.

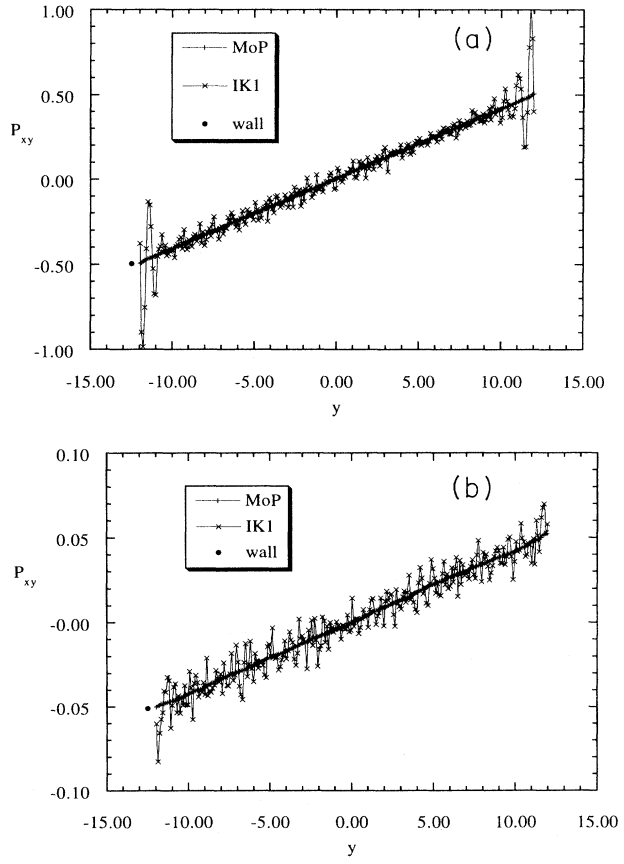

FIG. 5. P_{xy} calculated by IK1, MOP, and at the walls. (a) $\bar{n}=0.8362$; (b) $\bar{n}=0.4181$.

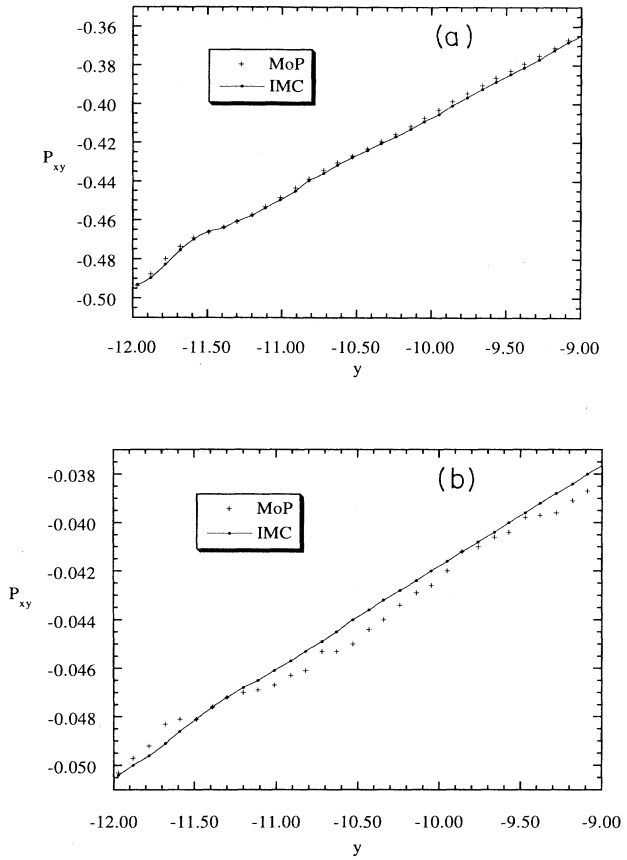

FIG. 6. Comparison of P_{xy} near wall for MOP and IMC. (a) $\bar{n}=0.8362$; (b) $\bar{n}=0.4181$.

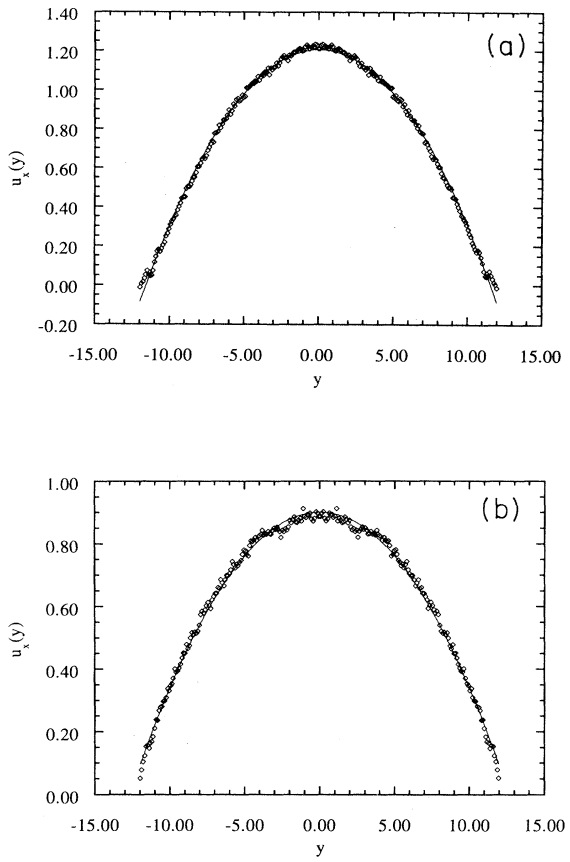

FIG. 8. Symmetrized streaming velocity profiles. (a) $\bar{n}=0.8362$; (b) $\bar{n}=0.4181$.

pore width of 10. In this narrow pore the oscillations are quite pronounced. We can also see that there is excellent agreement between the shear stress computed using the MOP and IMC techniques. That these two quite different techniques show the same oscillations confirms that the oscillations are not an artifact. This has important consequences, as it implies that the viscosity near the walls is not uniform (as is assumed in continuum hydrodynamics) but oscillates as a function of y. The magnitude of the effect increases as the pore width decreases. We are aware of at least one other group that has theoretically predicted this oscillatory behavior in the viscosity close to the walls [16], and this interesting phenomenon is currently the subject of further investigation by both groups.

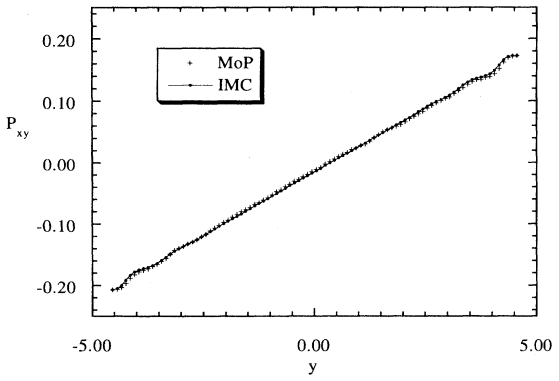

FIG. 7. P_{xy} calculated by IMC and MOP for a pore width of $l_y=10$; $\bar{n}=0.84$, $\bar{T}=0.91$.

It is important to appreciate that use of the IK1 procedure will generate incorrect results in regions where the density oscillates on atomic length scales. For instance, Thompson and Robbins [17], in calculating the shear stress for a Lennard-Jones fluid undergoing Couette flow, find that it exhibits oscillations that are correlated with the density oscillations. This they say cannot be understood in terms of the macroscopic equations of hydro-

TABLE III. Second-order polynomial coefficients for the streaming velocity profile. c_n is the coefficient of the nth-order term in the expansion. Since the velocity profile is symmetric about $y=0$, only even order terms for the polynomial expansions are considered.

$\bar{n}$	c_0	c_2
0.8362	1.2066	-9.0142×10^{-3}
0.4181	0.9010	-5.6106×10^{-3}

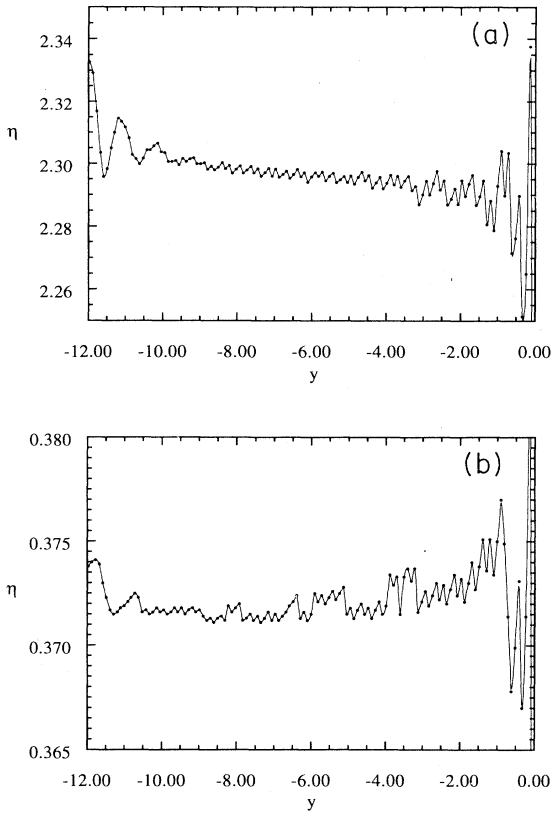

FIG. 9. Symmetrized viscosity profiles calculated by IMC. (a) $\bar{n}=0.8362$; (b) $\bar{n}=0.4181$.

dynamics because these are derived assuming quantities are averaged over scales larger than the mean free path. This is certainly true for the case of the Navier-Stokes equations, but applying the IMC technique to their Couette flow geometry will yield a constant value for the shear stress. Although they do remove these oscillations by appropriate averaging, they do not indicate how they calculated the shear stress. It is suspected that they used the IK1 expression, which would result in artificial oscillations similar to those reported in this paper. Use of IK1 would mask any genuine oscillations which might be found in the shear stress, such as those reported in this paper for Poiseuille flow.

From Eq. (37) we see that $\eta(y)$ is a function of $P_{xy}(y)$ and the strain rate $\gamma(y)$. The strain rate $\gamma(y)$ is found by differentiating the observed velocity profile $u_x(y)$, which itself is determined by binning the velocity data. Each bin has a volume V_{bin}. We then fit a polynomial to the binned data. Continuum hydrodynamics predicts a symmetric second-order polynomial for the streaming velocity profile, as described by (39). However, this solution relies upon the assumption of constant viscosity, which as we have seen is not necessarily true for narrow pores.

We fit the velocity profile to a set of four symmetric polynomials of second, fourth, sixth, and eighth order. Perhaps surprisingly, it turns out that the best fit to $u_x(y)$ is in fact given by a second-order symmetric polynomial. Further work has confirmed this down to pore widths as narrow as 5 atomic diameters. Figure 8 shows a comparison of the binned velocity data and the best quadratic fit to that data for the two systems. Once again we have symmetrized the data to improve statistics. Table III shows the coefficients of these polynomials.

In Fig. 9 we plot symmetrized viscosities calculated via the IMC method for both densities. Caution needs to be taken in interpreting the results near the center of the pore. Because the strain rate is zero at the center of the pore the signal-to-noise ratio must go to zero there and the *computed* viscosity must diverge to plus or minus infinity in this region.

In Fig. 9(a) we observe two interesting features of the viscosity profile for $\bar{n}=0.8362$. First, there is a gradual increase in the viscosity from the center of the pore to the walls. This trend in the viscosity mirrors that observed in the density profile and is a consequence of the nonuniform temperature profile of the fluid, which is maximum at the center of the pore and a minimum at the walls. To check that this was the case, a separate equilibrium simulation at constant fluid temperature was performed, and it was seen that the average density (and hence average viscosity) remained constant throughout the fluid.

Even more interesting in our results are the weak oscillations in $\eta(y)$ near the walls. These oscillations are strongest at the walls and grow progressively weaker towards the center of the pore, and are the result of fluid layering.

Figure 9(b) shows the corresponding viscosity profile for the case of $\bar{n}=0.4181$. Again the viscosity near the center of the pore is inaccurate for the reasons given above. The statistical uncertainties are so large that we cannot be certain whether or not there is a gradual increase in $\eta(y)$ as we move towards the walls. At this much lower density we might expect that this gradual wall enhancement of the viscosity may be very weak. This is expected since the density oscillations shown in Fig. 3(b) are also weaker than those in the higher density Fig. 3(a).

Finally, we can determine an effective continuum hydrodynamic viscosity by the application of (41). This gives a value of $\bar{\eta}=2.32$ for $\bar{n}=0.8362$, and $\bar{\eta}=0.37$ for $\bar{n}=0.4181$.

V. CONCLUSIONS

In this paper we have presented an alternative statistical mechanical derivation of the pressure tensor. The derivation avoids the mathematically awkward Taylor series expansion of delta function differences that is used in the original Irving-Kirkwood derivation. The derivation also avoids heuristic notions of the force "across" a unit area.

We show that as a direct consequence of the following three equations,

$$\rho(\mathbf{k},t)\equiv\sum m e^{i\mathbf{k}\cdot\mathbf{r}_i} , \tag{42a}$$

$$\mathbf{J}(\mathbf{k},t)=(i\mathbf{k}i\mathbf{k})^{-1}\cdot i\mathbf{k}\dot{\rho}(\mathbf{k},t) , \tag{42b}$$

$$\mathbf{P}(\mathbf{k},t)=(i\mathbf{k}i\mathbf{k})^{-1}\cdot i\mathbf{k}\dot{\mathbf{J}}(\mathbf{k},t) , \tag{42c}$$

one obtains the standard IK expression for the pressure tensor. We show that these equations also lead directly to a pressure tensor that can be simply interpreted as the force "across" a unit area, and leads to our method of planes for calculating the pressure tensor. Equations (42) *define* the Irving-Kirkwood gauge for hydrodynamic densities, $\mathbf{J}, \mathbf{P}, \ldots$.

The MOP includes an exact summation of the infamous O_{ij} operator expansion and unlike the IK expression is simple to implement in practice. In numerical calculations of the variation of the pressure tensor across a slit pore, we find that MOP is more accurate and computationally efficient than the approximate IK1 method (i.e., IK employing the approximation that $O_{ij}=1$).

For the special case of Poiseuille flow we compare the MOP estimate for the pressure tensor with a mesoscopic integration of the momentum continuity equation. In our IMC method we resolve the ambiguity in the hydrodynamic definition of the pressure tensor through the assumption that the shear stress is zero when the strain rate is zero.

This can easily be shown to be equivalent to the IK gauge when we observe that if the external field is added to the equation for the pressure tensor and we assume the flow is steady, we find that

$$P_{xy}(k_y,t)=-ik_y n(k_y,t)F_e/k_y^2 \ . \tag{43}$$

[We note that although in this case $(\mathbf{kk})^{-1}$ does not exist, $(\mathbf{kk})^{-1}\cdot\mathbf{k}$ is finite.] From (43) we can easily show

$$P_{xy}(y,t)=-F_e \sum_{i=1}^{N} \mathrm{sgn}(y_i-y)/2A \ . \tag{44}$$

This equation is the exact statistical mechanical analog of the IMC equations (30) and (31). Thus the IMC gauge and the IK gauge are identical for Poiseuille flow.

For simulated Poiseuille flow in a narrow slit pore the IMC and MOP calculations of the shear stress exhibit remarkable numerical agreement. This agreement is even observed in very narrow slit pores where the shear stress exhibits oscillations that reflect the effects of fluid atoms packing against the walls.

ACKNOWLEDGMENTS

We would like to thank Professor Keith Gubbins for valuable discussions and cooperation throughout this work. We also thank the Australian National University Supercomputer Facility for a substantial allocation of computer time.

[1] J. H. Irving and J. G. Kirkwood, J. Chem. Phys. **18**, 817 (1950).
[2] P. Schofield and J. R. Henderson, Proc. R. Soc. London Ser. A **379**, 231 (1982).
[3] R. Lovett and M. Baus, Physica (Amsterdam) **194A**, 93 (1993).
[4] A. Harasima, Adv. Chem. Phys. **1**, 203 (1958).
[5] M. Rao and B. J. Berne, Mol. Phys. **37**, 455 (1979).
[6] S. J. Hemingway, J. R. Henderson, and J. S. Rowlinson, Faraday Symp., Chem. Soc. **16**, 33 (1981).
[7] J. P. R. B. Walton, D. J. Tildesley, J. S. Rowlinson, and J. R. Henderson, Mol. Phys. **48**, 1357 (1983).
[8] D. J. Lee, M. M. Telo da Gamma, and K. E. Gubbins, Mol. Phys. **53**, 1113 (1984).
[9] M. J. Haye and C. Bruin, J. Chem. Phys. **100**, 556 (1994).
[10] D. J. Evans and G. P. Morriss, *Statistical Mechanics of Nonequilibrium Liquids* (Academic, London, 1990).
[11] D. J. Evans, Phys. Rev. A **23**, 2622 (1981).
[12] J. D. Weeks, D. Chandler, and H. C. Andersen, J. Chem. Phys. **54**, 5237 (1971).
[13] J. G. Powles, S. Murad, and P. V. Ravi, Chem. Phys. Lett. **188**, 21 (1992).
[14] S. Y. Liem, D. Brown, J. H. R. Clarke, Phys. Rev. A **45**, 3706 (1992).
[15] A. Baranyai, D. J. Evans, and P. J. Daivis, Phys. Rev. A **46**, 7593 (1992).
[16] K. E. Gubbins (private communication).
[17] P. A. Thompson and M. O. Robbins, Phys. Rev. A **41**, 6830 (1990).